Original Research Article: full paper

(2022), «EUREKA: Physics and Engineering»
Number 6

# NUMERICAL SIMULATION OF THE INLET CHANNEL GEOMETRY INFLUENCE IN THE TORQUE GENERATED AT THE GRAVITATION WATER VORTEX TURBINE

***Andres Burbano***
*Department of Mechatronics Engineering[1]*

***Jorge Sierra***✉
*Department of Mechatronics Engineering[1]*
*Department of mechanical Engineering[2]*
*jorgesierra@itm.edu.co*

***Edwin Correa***
*Department of Mechatronics Engineering[1]*

***Alejandro Ruiz***
*Department of Mechatronics Engineering[1]*

***Daniel Sanin***
*Department of Engineering[3]*

*[1]Research Group – MATyER*
*Instituto Tecnologico Metropolitano*
*Cl. 75#75-10 Medellín, Colombia, 050035*

*[2]Research Group – GIIAM*
*Institucion Universitaria Pascual Bravo*
*Cl. 73#73a-226 Medellin, Colombia, 050041*

*[3]Research Group – GIIEN*
*Institucion Universitaria Pascual Bravo*
*Cl. 73#73a-226 Medellin, Colombia, 050041*

✉**Corresponding author**

**Abstract**

The gravitational water vortex turbine is presented as an alternative for electric power generation for both low head and water flow conditions, additionally it is easy and low cost to implement and maintenance. However, the experimentally reported efficiencies motivate the scientific community to develop new geometries in order to improve its performance. First, it is not clear how the efficiency of the turbine is obtained and second, not all studies report it. The turbine is mainly made up of a tank, the rotor and the electric generator. The geometry of the tank is important because it stabilizes the fluid and in this component that the generation of the vortex is induced, which determines, added to other factors like tank geometry and runner, the global efficiency of the turbine. The primary purpose of this study is to compare numerically the torque generated at six (6) geometrical configurations of the basin inlet channel for Gravitational Vortex Turbine (GVT) with a Savonius rotor. The study was developed in ANSYS® CFX, where a transient state VOF model was configured with a BSL *K*-ω turbulence model and a discretization a discretization of the control volume made in the ICEM module. The highest torque was 0.553 Nm at 25 rpm for the trapezoidal curved inlet channel geometry, increasing the efficiency respect to the conventional Square inlet channel of the 2.73 %. The increase of tangential velocity contributes positively to the vortex generation, and consequently, an increase in torque is obtained. On the other hand, the design of the rotor considerably affects the performance of the GVT, where it may or may not take advantage of the kinetic energy of the vortex.

**Keywords:** vortex, geometry, turbine, energy, basin, inlet-channel, CFD, runner, torque, performance.

**DOI: 10.21303/2461-4262.2022.002703**

## 1. Introduction

Over the years, global warming has caused an increase in $CO_2$ and the use of fossil fuels has increased and caused aggravation in our ecosystem; therefore, the demand for renewable energy has been of significant impact on reducing pollutants from the burning of fossil fuels. For this reason, hydropower is a strong alternative and is expected to be one of the pillars of renewable energies [1]. However, hydropower generation is mainly a large-scale centralized type using a turbine with a relatively large head. The most commonly used turbines for this type of hydropower are Francis turbines [2] and Propeller turbines. However, sometimes the space required to construct this type of hydroelectric power plant is larger. Therefore, lately, the studies of small-scale hydroelectric generation have taken force with alternatives for power generation from river water and irrigation canals using a turbine in an open channel [3−5]. For this reason, it has been focused on Gravitational Water Vortex Turbine (GVT) [6], which is used in a small-scale hydropower generation system; this type of hydropower generation system adopts as name Gravitation Water Vortex Power Plant [7].

The GVT is classified as an ultra-low head micro hydropower system that operates in 0.7−2 m [8] and does not require a substantial reservoir or installation area [9]. Water from streams, coastal currents, or riverbanks is channelled into a vertical pool with a circular cross-section known as a basin and a small outlet at the bottom to generate a water vortex under gravity in a GVT [10]. A powerful vortex forms in the basin due to localized pressure at the basin orifice, induced tangential velocity, and circulation created by the deflector in the upstream channel. The created vortex's velocity is made up of axial, radial, and tangential components [11]. A co-axial gravitational water vortex turbine will generate power from an artificially induced vortex [12]. For low head sites, conventional turbines such as the Pelton and Kaplan turbines can be scaled down but still, appropriate flow rates are required, which necessitates a larger-than-average size, raising the cost [13–15]. As a result, compact hydraulic turbines such as the GVT must be designed to capitalize on the potential of low-head and low-flow-rate water [16, 17]. The vast potential of hydro energy has remained untapped due to a lack of potential heads [18]. Unlike the Pelton turbine, the GWVT has all its blades in contact with water simultaneously.

Furthermore, in GWVT, water impinges on the entire circumferential area, exerting forward push force in contrast to reaction turbines (Francis and Kaplan); while sliding over the blades, the water exerts a reaction force. As a result, the effective area of the blade in the former type of turbine is greater than that in the latter. Because of its high work potential, it is an excellent candidate for the application of micro-hydropower plants (MHPPs) [19].

In the GVT, two fundamental components have been studied in recent years: the basin, and the rotor. For the rotor studies, [20] published the first paper on turbine development for the GVTs. Different sizes of Francis turbines at various depths were examined using simulation to assess the impacts of the basin shape on GVT performance. It was determined through numerical simulation, and theoretical modeling that the vortex created was proportional to the rotational speed. The presence of the turbine was also found to dramatically lower vortex height while diminishing GVT efficiency. The performance of GVT reduced as the number of custom-designed turbine blades increased from six to twelve [21]. However, a study [13] found the opposite; increasing the number of turbine blades from two to four improved GVT performance. Such findings suggested the possibility of an appropriate number of blades for the GVT turbine. The conclusions also likely differ due to differences in turbine design, with [21] employing curved and flat blades. In addition to the contrary finding, [21] reported that the best-recorded efficiency of 15.1 % was attained using two turbines with huge blade sizes. According to them, the resistance force required to stop the turbine with a large blade was more remarkable, increasing the turbine's power output. A study [22] investigated the optimization of three runners to improve the efficiency of the GVT; straight, twisted, and curved blade profiles were used in the study; the results revealed that the curved blade profile has the highest peak efficiency of 82 %, compared to 46 % for the straight runner and 63 % for the twisted runner. Another important study parameter for implementation is the application of rotor materials [23] investigated the effect of turbine materials on the efficiency of power generation from a water-free vortex hydropower plant composed of steel and aluminium. The results showed

that steel and aluminium turbines' highest power generation efficiency was 33.56 % and 34.79 %, respectively. The torque value and power generation efficiency of the aluminium turbine was found to be higher than that of the steel turbine at an average of 8.4 % and 8.14 %, respectively, at the maximum water flow rate of 3.63 $m^3$/min. This result demonstrated that the water turbine's lightweight might improve torque and power generation efficiency.

Under the advanced turbine development, some studies focused mainly on the basin giving several alternatives to work together on the turbine developments, e.g., a study [24] used three alternative basin designs in their simulations. Due to its high capacity to deliver consistent velocity determined that a cylindrical basin with an inlet guide was ideal [19] conducted a CFD simulation to perform a numerical analysis of the basin's geometry. Tangential velocity increased with creating an air-core in the water vortex, they discovered. Furthermore, the tangential velocity was highest when the water level in the basin was slightly higher than the water level, and the basin's diameter was increased to some extent [21] predicted that a conical basin enhances the intensity of the vortex. The results indicated that the conical basin had a maximum efficiency of 29.63 %, much higher than the values obtained from all cylindrical basin experiments. For the production of a strong vortex, the ideal orifice diameter to uniform basin diameter ratio is between 0.14 and 0.18 [25]. One study [26] investigated concave and convex tank designs for gravitational vortex turbines numerically and experimentally. The numerical results suggest that the outflow velocity of the convex design increases from 1.12 m/s to 1.81 m/s. These data indicate a 62 % increase in the concave design's outlet velocity over the convex configuration. However, experimental data suggest that concave designs create more electrical power (0.37 W) than convex designs (0.23 W). These empirical findings indicate a 60 % increase in performance when comparing concave to convex designs.

In summary, none of the studies mentioned above have been modified the inlet channel or any other modification related to the channel, providing a study parameter for this new type of turbine with which fundamental data can be extracted for the GVT (Gravitational Vortex Turbine), which allows to create a structured model on the phenomena associated with the fluid velocity and how it affects the appropriate generation of the vortex in the basin area.

Therefore, for this study, the change of the inlet channel is designed by introducing three types of channels. First is the straight channel, this type of channel, together with the conventional (straight) are the most common channels used in the GVT. Second is a channel with a radius of 800 mm located in the deflector plate and third channel is a curved deflector plate that goes from the starting point of the channel inlet to the neck of the channel. In addition, two types of cross-sections were studied together with the combination of these types of channels to study in-depth the impact of the channel cross-section. First is the square cross-section which is the most common section used in the GVT and the second is a trapezoidal cross-section with these changes we seek an increase in the turbine torque by making changes in the geometry that alter the transport of the fluid velocity and also study the reduction of the inlet flow and how it impacts the generation of turbine power.

## 2. Materials and methods

### 2. 1. Research object

The present study used the finite volume method to simulate the flow in the basin, rotor, and velocity distribution in the plane where the turbine extracted the most power. The fluid flow domain was constructed in CAD software Space Claim, the mesh was done in ICEM. For simulation purposes, the model was imported into ANSYS Fluent, a commercial CFD code.

Six unique cases are defined for the square cross-section channel applying the three changes in the channel (straight channel, 800 mm radius channel, and curved channel), adding up to 3 unique cases, in the same way the previous condition applies for the trapezoidal section channel giving a total of 6 cases, **Fig. 1** shows the design parameters proposed in the study.

Each case is defined with an abbreviation mentioned in **Table 1** to identify and discuss results.

The rotor employed for the research was a Savonius-type rotor with two big cylindrical blades with concave and convex sides. This rotor type was chosen because the Savonius rotor operates by drag, as seen in **Fig. 2**.

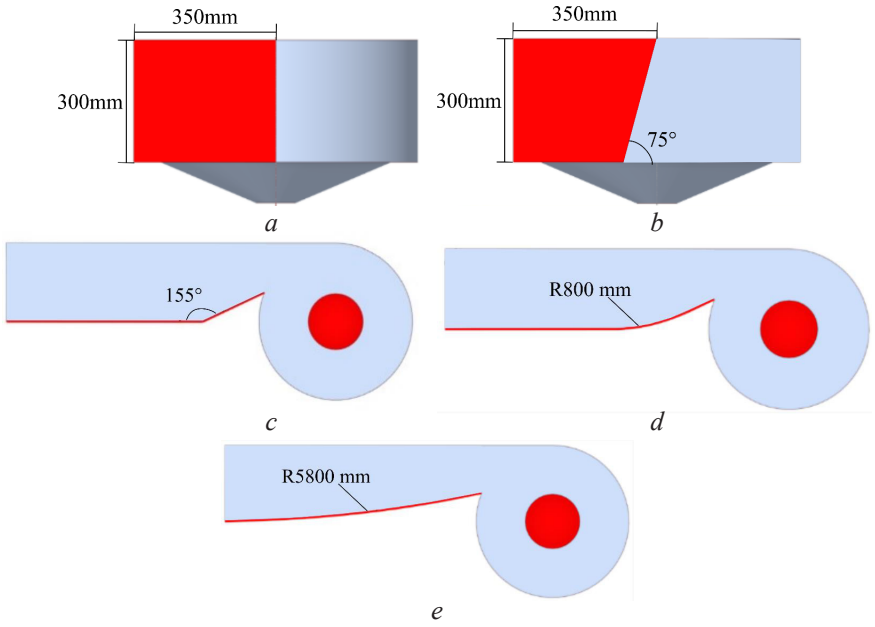


**Fig. 1.** Proposed design parameters: *a* − square cross-section modification; *b* − trapezoidal cross-section change; *c* − Standard straight channel; *d* − curved modification in the channel; *e* − Totally curved modification in the channel

**Table 1**
Channel definition for GVT

| Cross section | Channel type | Abbreviation |
|---|---|---|
| Square | Straight | *S-S* |
| | Curved ($r = 800$ mm) | *S-C* |
| | Totally curved | *S-T* |
| Trapezoidal | Straight | *T-S* |
| | Curved ($r = 800$ mm) | *T-C* |
| | Totally curved | *T-T* |

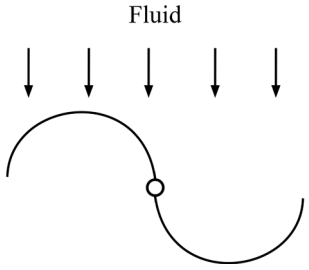


**Fig. 2.** Basic diagram of a Savonius rotor

Given the same surface area, the drag coefficient of a concave surface is substantially larger than that of a convex surface, according to basic physics principles. As a result, when the oncoming fluid contacts the rotor, the concave side encounters more significant drag than the convex side. This causes the rotor to rotate, hence driving the turbine. Since GVTs operate at relatively low flow rates, they have lower power coefficients than drag devices. Furthermore, Savonius rotors have high resilience and starting torque. Savonius rotors are ideal for increased torque, and low-speed applications due to these qualities [27].

**Fig. 3** shows the dimensions of the Savonius rotor used. A basic Savonius rotor was defined with no additional deflectors or blade positioning offset, i.e., both blades start at the zero

point (center) of the shaft, the radius of the rotor is 50 mm, and the blade height is 136 mm; as the rotor is positioned close to the exit hole, it is required that only a small section of the blades take advantage of the fluid velocity generated by the vortex as dictated by [28] in their study of the positioning of the rotors, with this it is ensured that only the water is impregnated with the highest velocity of the vortex generated at the exit of the system.

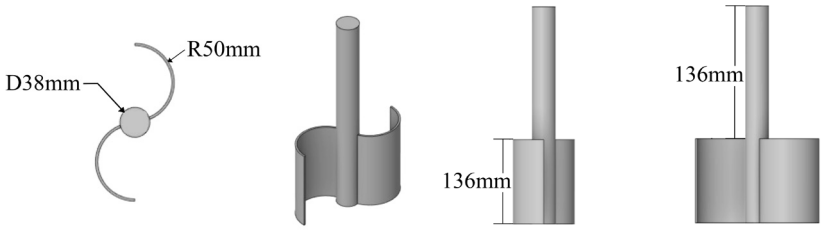


**Fig. 3.** Savonius rotor dimensions

**2. 1. Governing equation**

Computational Fluid Dynamics (CFD) is the technique of substituting discretized algebraic forms for the integrals/partial derivatives in fundamental fluid equations, which are then solved to get numbers for the flow field values at discrete points in time or space. All CFD codes consist of three fundamental components: a pre-processor, a solver, and a postprocessor [29, 30]. Since CFD software calculates the fluid variables, a mathematical model must approximate the result. For this, there are the Navier-Stokes equations. The following equations describe the continuity equation (1)−(4) in cylindrical coordinates:

$$\frac{\partial V_r}{\partial r}+\frac{\partial V_z}{\partial z}+\frac{\partial V_r}{r}=0, \tag{1}$$

$$V_r\left(\frac{\partial V_r}{\partial r}\right)+V_z\left(\frac{\partial V_\theta}{\partial z}\right)-\left(\frac{V_rV_\theta}{r}\right)=v\left(\frac{\partial^2V_\theta}{\partial r^2}+\frac{\partial V_\theta}{r\partial r}-\frac{V_\theta}{r^2}+\frac{\partial^2V_\theta}{\partial z^2}\right), \tag{2}$$

$$V_r\left(\frac{\partial V_r}{\partial r}\right)+V_z\left(\frac{\partial V_r}{\partial z}\right)-\left(\frac{V_\theta^2}{r}\right)+\left(\frac{\partial \rho}{\rho\partial z}\right)=v\left(\frac{\partial^2V_r}{\partial r^2}+\frac{\partial V_r}{r\partial r}-\frac{V_r}{r^2}+\frac{\partial^2V_r}{\partial z^2}\right), \tag{3}$$

$$V_r\left(\frac{\partial V_z}{\partial r}\right)+V_z\left(\frac{\partial V_z}{\partial z}\right)-\left(\frac{\partial \rho}{\rho\partial z}\right)=v\left(\frac{\partial^2V_z}{\partial r^2}+\frac{\partial V_z}{r\partial r}+\frac{\partial^2V_r}{\partial z^2}\right). \tag{4}$$

Tangential, radial, and axial velocity components are denoted by $V_\theta$, $V_r$ and $V_z$, respectively, while kinematic viscosity is denoted by $v$ [31]. It is impossible to obtain an analytical solution immediately due to the intricacy of the equations. As a result, CFD techniques are employed to approximate a solution to these equations.

**2. 2. Volume control**

A control volume with appropriate dimensions is introduced. The diameter of the Savonius rotor is 0.2 m. According to [26], the inlet and outlet boundary conditions have been adjusted. **Table 2** summarizes the geometrical characteristics of the control volume, and **Fig. 4** shows the control volume.

The simulation is performed with a constant inlet velocity (0.2 m/s) and is kept constant. The two boundary flow lines (i.e., the standard derivatives of the dependent variables are zero) are subject to the symmetry requirements of the boundary. In the rotating zone where the turbine is located, two interfaces are applied as a boundary condition to maintain the continuity of the flow field.

The blade surfaces are made of a non-slip material, **Fig. 5, 6** shows the boundary conditions of the channel and rotor control volume, respectively.

**Table 2**
Design parameters

| Parameter | Symbol | Value |
|---|---|---|
| Channel height | *Hc* | 0.3 m |
| Channel width | *Wc* | 0.35 m |
| Channel length | *Lc* | 1.5 m |
| Notch length | *Lr* | 0.9 m |
| Notch angle | *a* | 155° |
| Basin height | *Ht* | 0.4 m |
| Basin diameter | *Dt* | 0.7 m |
| Conical angle | *b* | 67° |
| Outlet | *Ds* | 0.090 mm |
| Diameter of rotary domain | *Dr* | 0.25 m |
| Height of rotary domain | *Hr* | 0.35 m |
| Turbine diameter | – | 0.2 m |
| Turbine height | – | 0.13 m |

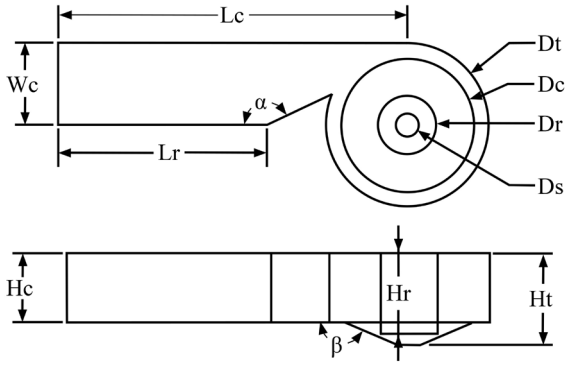


**Fig. 4.** Base GVT control domain

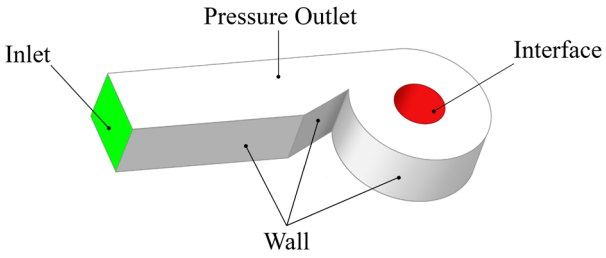


**Fig. 5.** Boundary conditions for channel control domain

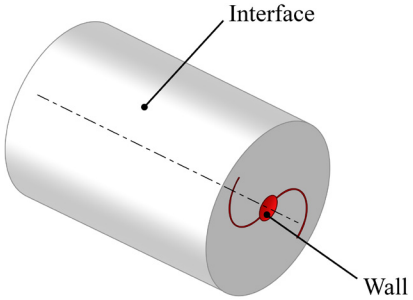


**Fig. 6.** Boundary conditions for rotor control domain

Since the model uses wall functions, a $y^+$ equal to 30 was defined to avoid conflicts when calculating near walls for $y^+$ numbers less than 30 [32].To calculate the height of the first mesh cell off the wall required to achieve the desired $y^+$ using flat-plate boundary layer theory is given by:

$$y = \frac{y^+ \mu}{\rho u^*}, \tag{5}$$

where $y^+$ value indicates the wall spacing in (m), dynamic viscosity μ (kg/ms), fluid density ρ (kg/m³), and dimensionless velocity $u^*$.

The sliding mesh method is used. Although the sliding mesh model is potentially the most realistic way of simulating rotating flows and can accurately depict the entire transient start-up, it is also the most computationally expensive. When this technique is applied to a specific scenario, it produces two distinct cell zones (the first one is a cylindrical cell containing the gear, the second one is the remaining volume). Each cell zone is separated from the adjacent cell zone by an interface. The two cell zones will move relative to one another in distinct increments along with the mesh interface. The selected grid type is the structured grid which consists of hexahedral elements adopted for both fixed and rotating flow domains. The structured grids are significantly increased to obtain a normalized wall distance in the vicinity of wall borders. The grid in the control domain is depicted in **Fig. 7**, and the quality of elements is given in **Table 3**.

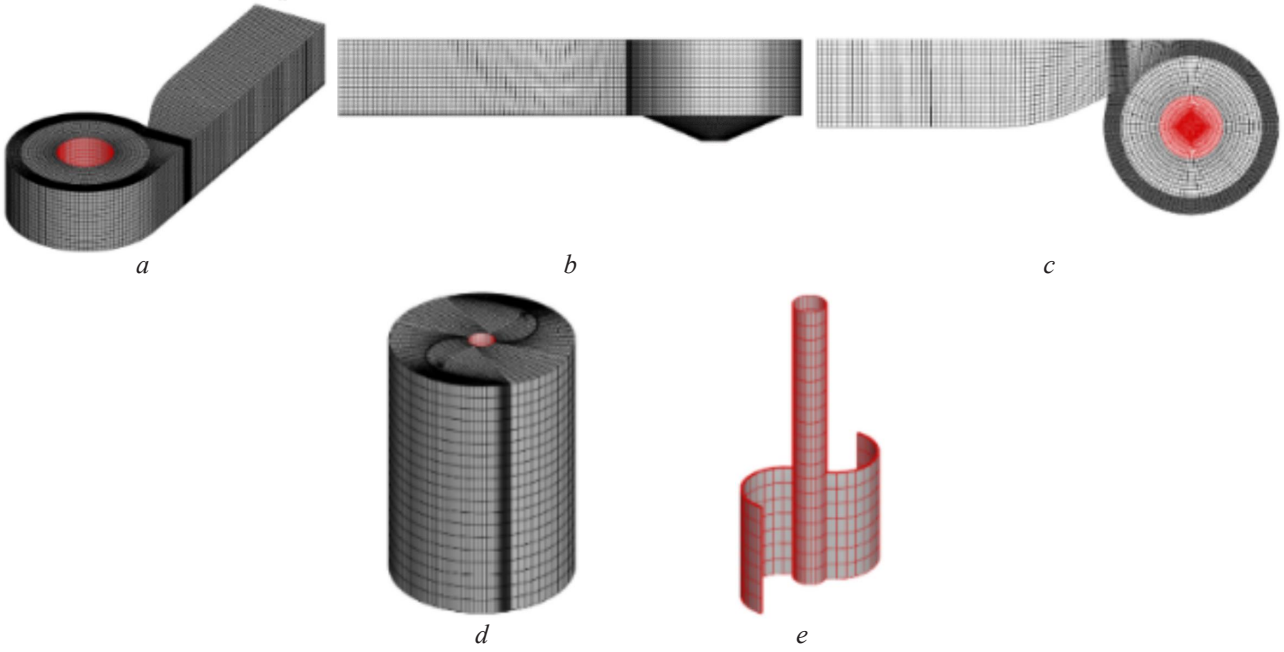


**Fig. 7.** Mesh on the control volume: *a* – isometric view of channel; *b* – front view of channel; *c* – top view of channel; *d* – isometric view of rotor control volume; *e* – Savonius rotor mesh

**Table 3**
Mesh quality metrics

| Quality criteria | Rotor | Channel |
|---|---|---|
| Min. Element quality | 0.613 | 0.632 |
| Max. Aspect ratio | 17 | 10 |

A mesh independence study was carried out to provide stability in the simulation of the cases; mesh independence is an important concept to grasp as it can be used to distinguish whether the solution obtained is independent of the mesh resolution. It also allows to ensure that results are achieving the optimal solution time, and not enlarging the mesh and solution times. Finding the

balance between mesh density and the final solution is crucially important to a CFD simulation and a mesh independence study is the first step to evaluating the accuracy of our results. The best method to implement a mesh independence check is to gradually refine and coarsen the mesh in the important regions refine and coarsen the mesh in the critical regions gradually, and then compare the results and plot the difference. Ideally, let's look to achieve a value that does not overly change without over-refining the mesh. The configuration was investigated using the S-S case since it will give an overview of the behaviour of the case in its base model and be able to use the information and apply it to the modifications previously identified by the study.

The mesh for both interface boundaries contains the same number of cell sizes to obtain a fast convergence in the continuity equation. The density of the structured elements in the 3D CFD domain were studied, and it is observed that the number of elements ranges from 5E4 to 8.5E5 elements. This study shows that number of elements larger than 2.3E5 lead to a relative variance of 1.9 %. Therefore, a mesh consisting of 2.5E5 to 3.5E5 elements was defined for all subsequent simulations to save time and reduce the computational cost. **Fig. 8** shows the mesh independence study.

The effect of 4 turbulence models has been investigated and reported quantitatively, *k-w* BSL [31], SST *k-w* [32], realizable *k-e* [33], and Reynolds Stress BSL [34]. **Fig. 9** shows the curves of the four proposed turbulence models. The *k-w* model was selected because the quantitative comparison of the torque generated by the Savonius rotor vane number 1 was performed; the results showed that the *k-w* BSL model presents very few discrepancies in the behaviour of the torque compared to the other three turbulence models, highlighting that the Reynolds Stress model has the highest accuracy of the four models, the relative error value between the *k-w* BSL and the Reynolds Stress BSL was 2.482 % giving reliability in the results of the proposed case. In addition, this technique offers very good convergence. The *k-w* model does not depend directly on arbitrary values of free flow and does not require high demand in terms of computational calculation.

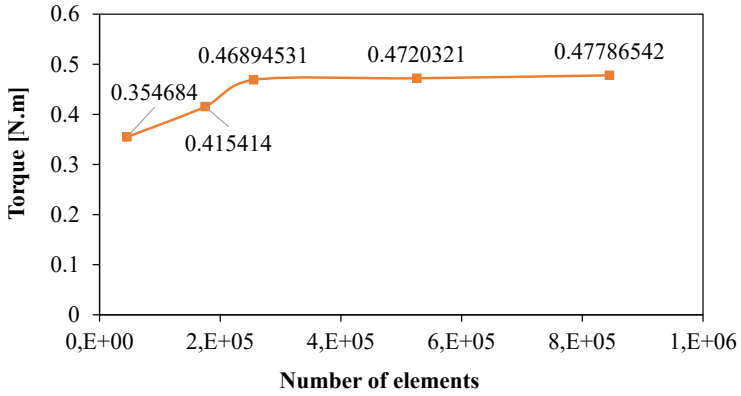


**Fig. 8.** Mesh Independence study

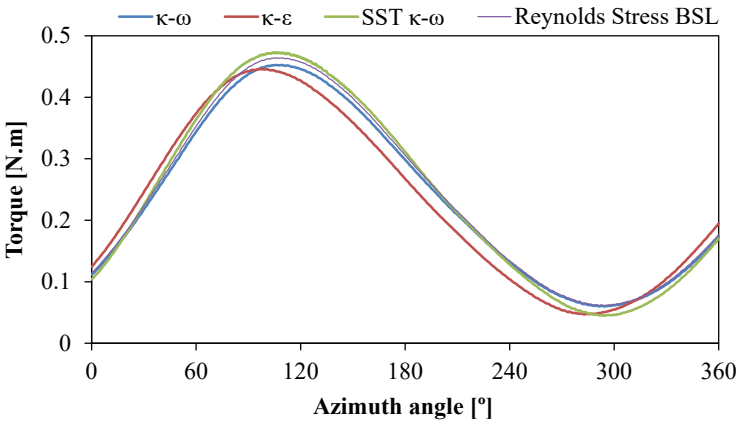


**Fig. 9.** Effect of different turbulence models in the torque results for the *S-S* case

The method of selection and calculation of time step was adopted from the study published by [33]; it is found that the variation of the time step depends directly on the TSR value of the turbine; for a higher TSR the time step will be reduced, The tip speed ratio (TSR) is a ratio of the tip blade velocity ω*R* velocity of the fluid, and this ratio is defined as the (6).

$$\mathrm{TSR} = \frac{\omega R}{\vartheta}. \tag{6}$$

Where ω is the rotational velocity, *R* is the rotor radius, and *V* is the fluid velocity for this study was calculated for a total of 15 s a time step size of 0.007 s ensuring that the turbine advances 1° for each time step giving greater accuracy and ease when performing the analysis of the torque.

The convergence conditions were set to obtain a periodic variety of torque and satisfy a maximum residual value of 1e-06. Finally, the torque value for the 2-bladed rotor was set and reported to determine the maximum power of the Savonius rotor. **Table 4** summarises the boundary conditions of the case. The VOF method was used for all cases, and it is provided by ANSYS Fluent, the transient surface tracking technique designed for two or more immiscible fluids where the position of the phase-phase interface is of interest in this case, the interaction between water and ambient air. In the VOF model, a single set of mixing momentum and energy equations is shared between the basin and rotor phases, finally being solved implicitly. When applying the VOF model, an interaction between the two fluids with a surface tension equal to 0.072 N/m was performed to simulate the ambient temperature.

**Table 4**
Grid and boundary conditions

| Parameter | Description |
|---|---|
| Interface/Type | Sliding/Conformal |
| Grid/Type | Structured/Hexa |
| Model | Volume of fluid (VOF) |
| Elements | 250,000–350,000 |
| Fluid | Air/Water |
| Turbulence Model | BSL *K*-ω |
| Inlet | Velocity Inlet |
| Outlet | Pressure Outlet |
| Blades | No-slip moving wall (ω = 0)rad/s |
| Residuals RMS criteria | 1E6 |
| Time | Transient |
| $Y^+$[–] | 30 |
| Free stream velocity [m/s] | 0.2 |
| Time Step Size [s] | 1° for each time-step |

### 2. 3. The impact of the rotational speed on the torque *T*

**Fig. 10** shows the torque variation as a function of the rotational speed of the rotor in the *S*-*S* case; the speeds were changed in an ascending way from 0 rpm to 150 rpm. It is possible to observe that the rotor obtains a maximum torque value for lower RPM; in the case of the maximum torque value, it is presented that when the rotor acquires a speed of 25 RPM, its torque value corresponds to 0.4681 Nm and decreases as the rotation speed increases for a speed of 150 RPM the torque value is 0.301 Nm, reducing the torque generated by a value of 35.6 %. Therefore, for the study, it was considered a rotational speed of the rotor at 25 rpm for all cases.

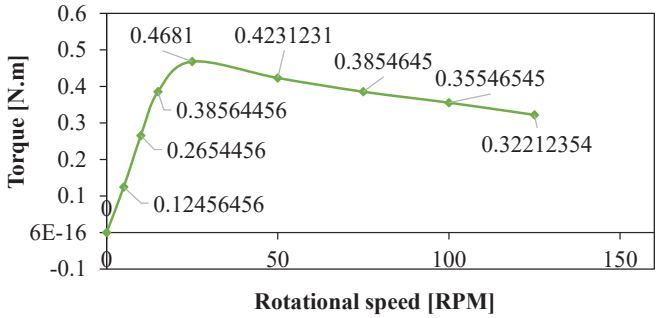


**Fig. 10.** Output torque values as function of RPM

## 3. Results and discussion

### 3. 1. The impact of the cross-sectional area on the blade No. 1 torque *T*

**Fig. 11** represents the torque variation in blade number 1 as the azimuth angle changes with respect to the initial position of the turbine; the torque data is extracted from the last turn, it is observed that the torque variation patterns for the square cross-section channel and the trapezoidal cross-section channel are similar from one to the other, This behaviour is expected because the turbine conditions are the same. No change was made for this type of parameter; these data suggest that for both cases, the torque value is similar for the square cross-section flume, the average torque value is 0. 2369 Nm, and the average value of trapezoidal cross-section is 0.2409 Nm, it is highlighted for both data the increase in the average torque value for the trapezoidal cross-section channel by 1.65 %.

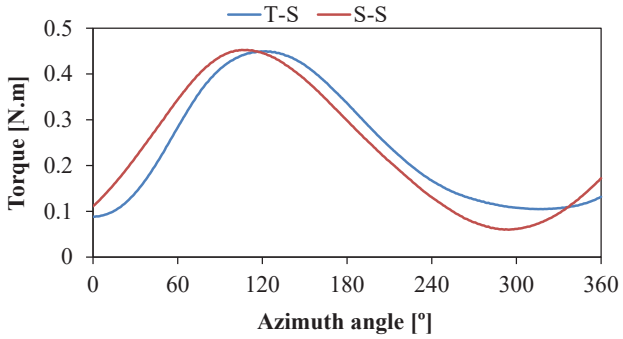


**Fig. 11.** Variation on torque of blade N°1

**Fig. 12** shows the velocity contours in both channels, the increase in torque is mainly since the trapezoidal section channel has a high ratio between the flow area and the area of contact with the wall. Consequently, the effect of the viscous forces on the flow velocity of the water is reduced, making the fluid move faster, helping the generation of the vortex to form quickly, and increasing the tangential velocity in the basin area.

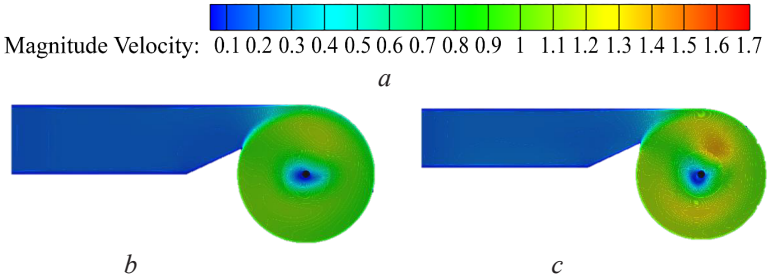


**Fig. 12.** The contour of the velocity magnitude: *a* – square cross-section; *b* – trapezoidal cross-section

### 3. 2. The effect of the channel modifications on the average torque $A_T$

**Fig. 13** shows the variation of the average torque of the turbine as a function of the azimuth angle; the graph represents the middle torque generation given by blade one and blade two of the Savonius turbine. It highlights two different behaviours regarding the square cross-section channel compared to the trapezoidal section. The first difference is the torque generation for the angles between 0° and 100°, representing average values for the square cross section channel with a value of 0.457 Nm instead of the trapezoidal channels with a value of 0.430 Nm; this is due to the generation of the vortex for this angle of attack; since the square channel has a lower tangential velocity for the generation of the vortex, the turbine blades are permeated with a more significant amount of the water surface as shown in **Fig. 14**. However, this behaviour decreases as the angle of attack increases; this behaviour decreases as the turbine advances in the azimuth angle; this is because the air core of the square channel is not wide enough so that the fluid does not continue to accelerate and consequently, the maximum torque is reached when the turbine has an azimuth angle equal to 156.96°.

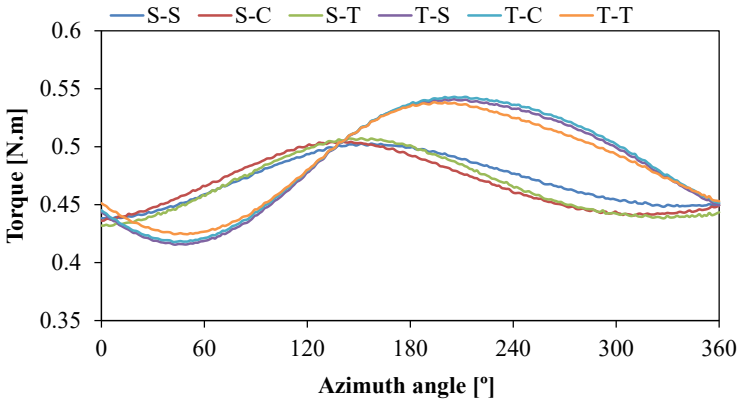


**Fig. 13.** Average torque output $A_T$

On the other hand, the behaviour of the trapezoidal flume stands out for its range of effectiveness for the generation of maximum torque; the torque range in the trapezoidal flume is between 150° and 300°; in this section of the azimuth angle, the turbine generates up to 0.526 Nm of nominal torque exceeding by 1.5 times the effective range for the case of square channels, this reason is due to the rotational speed of the fluid when it crosses the channelling zone towards the chamber, the highest the fluid velocity on the walls of the basin, the greater the air core of the vortex, and consequently the fluid-blade impact velocity will be generated with greater force producing a greater torque gain.

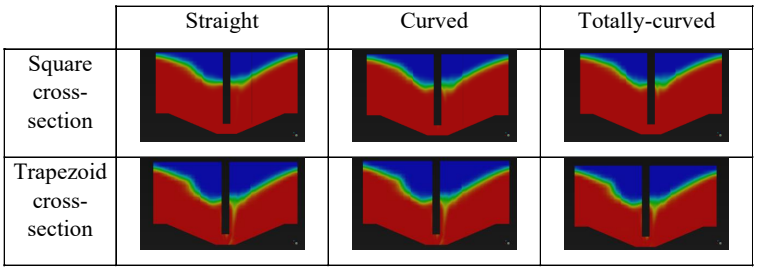


**Fig. 14.** Water volume fraction on the basin

Table 5 shows the results of the total torque generated, the maximum torque achieved by each type of channel, and the torque gains in percentage. It should be noted that for the square cross-section channels, no torque gain is obtained. On the contrary, a decreasing performance is obtained, this may be since the geometric modifications in the channel do not help the fluid to increase its speed towards the basin area, and therefore it is not used in a better way compared to the trapezoidal cross-section channel, The main reason is that with the change in cross-section and the

modifications to the channel, the incoming flow rate between the channel connection and the basin increases, generating a narrowing which is used by the basin, inducing an acceleration in the fluid and contributing to the generation of a pronounced vortex.

**Table 5**
Average T and max values for the turbine (Where Tp is the torque increase in %)

| Parameter | *S-S* | *S-C* | *S-T* |
|---|---|---|---|
| $T_p$ (%) | 0 | −0.686 | −0.938 |
| $A_T$ (Nm) | 0.469 | 0.466 | 0.465 |
| Max (Nm) | 0.510 | 0.508 | 0.507 |
| – | *T-S* | *T-C* | *T-T* |
| $T_p$ (Nm) | 2.41 | 2.73 | 2.07 |
| $A_T$ (Nm) | 0.480 | 0.482 | 0.479 |
| Max(Nm) | 0.553 | 0.55 | 0.542 |

The most studies on GVT have been presented for the design of the tank geometry or a specific geometric parameter. Therefore, there is no study showing the impact of two or more geometric parameters together on the GVT performance. Due to the above, it is not easy to determine which parameters considerably affect the formation of the vortex in the turbine. Thanks to an exhaustive analysis of the literature, it was possible to establish the parameters that can affect the formation of the vortex in a considerable way. However, it should also be aware that there are still parameters that directly affect the performance of the GVT, such as the rotor design. Therefore, it is expected that this study will be considered as a point of comparison for future work on gravitational vortex turbine performance.

## 4. Conclusions

This study aims to perform an analysis of the torque value of a GVT by making changes in the geometric parameters focused mainly on the inlet channel, the cross-section of the channel was modified, and curvatures were added in the deflector part of the channel to study its behaviour, also for this analysis let's evaluate the data about the torque extraction quantitatively for this type of GVT, the results of the study revealed: The increase of tangential velocity contributes positively to the vortex generation, and consequently, an increase in torque is obtained.

The change in the cross-section of the channel positively influences the torque report because the use of trapezoidal channels provides a decrease in the effect of viscous forces on the fluid velocity, which causes it to accelerate. The change in the geometric parameters in the baffle zone is positive only for the trapezoidal section channel because it generates a narrowing in the connection between the channel and the basin, which helps the fluid increase its velocity when entering the basin. The maximum torque gain that can be obtained compared to the conventional type of channel is 2.73 %. Based on the results, the trapezoidal cross-section channels applied in all cases are the most recommendable for their application; the increase for the 3 cases was more than 2 %.

## Conflict of interest

The authors declare that there is no conflict of interest in relation to this paper, as well as the published research results, including the financial aspects of conducting the research, obtaining and using its results, as well as any non-financial personal relationships.

## Acknowledgments

The authors are very grateful to Computación Avanzada y Diseño Digital (CADD) research line, which belongs to the Materiales Avanzados y Energía (MATyER) research group of Instituto Tecnológico Metropolitano (ITM), for providing the necessary equipment to carry out the numerical study of the present investigation.

**References**

[1] Pérez-Sánchez, M., Sánchez-Romero, F., Ramos, H., López-Jiménez, P. (2017). Energy Recovery in Existing Water Networks: Towards Greater Sustainability. Water, 9 (2), 97. doi: https://doi.org/10.3390/w9020097

[2] Liu, S., Zhang, L., Wu, Y., Luo, X., Nishi, M. (2006). Influence of 3D Guide Vanes on the Channel Vortices in the Runner of a Francis Turbine. Journal of Fluid Science and Technology, 1 (2), 147–156. doi: https://doi.org/10.1299/jfst.1.147

[3] Capecchi, D. (2013). Over and Undershot Waterwheels in the 18th Century. Science-Technology Controversy. Advances in Historical Studies, 2 (3), 131–139. doi: https://doi.org/10.4236/ahs.2013.23017

[4] Anyi, M., Kirke, B. (2010). Evaluation of small axial flow hydrokinetic turbines for remote communities. Energy for Sustainable Development, 14 (2), 110–116. doi: https://doi.org/10.1016/j.esd.2010.02.003

[5] Furukawa, A., Watanabe, S., Matsushita, D., Okuma, K. (2010). Development of ducted Darrieus turbine for low head hydropower utilization. Current Applied Physics, 10 (2), S128–S132. doi: https://doi.org/10.1016/j.cap.2009.11.005

[6] Nishi, Y., Inagaki, T. (2017). Performance and Flow Field of a Gravitation Vortex Type Water Turbine. International Journal of Rotating Machinery, 2017, 1–11. doi: https://doi.org/10.1155/2017/2610508

[7] Zotlöterer, F. (2004). Hydroelectric Power Plant.

[8] Application Area. Available at: http://www.zotloeterer.com/welcome/gravitation-water-vortex-power-plants/application-area/ Last accessed: 02.06.2021

[9] Wanchat, S., Suntivarakorn, R. (2012). Preliminary Design of a Vortex Pool for Electrical Generation. Advanced Science Letters, 13 (1), 173–177. doi: https://doi.org/10.1166/asl.2012.3855

[10] Gheorghe-Marius, M., Tudor, S. (2013). Energy Capture in the Gravitational Vortex Water Flow.

[11] Marian, M. G., Sajin, T., Azzouz, A. (2013). Study of Micro Hydropower Plant Operating in Gravitational Vortex Flow Mode. Applied Mechanics and Materials, 371, 601–605. doi: https://doi.org/10.4028/www.scientific.net/amm.371.601

[12] Rahman, M. M., Tan, J. H., Fadzlita, M. T., Wan Khairul Muzammil, A. R. (2017). A Review on the Development of Gravitational Water Vortex Power Plant as Alternative Renewable Energy Resources. IOP Conference Series: Materials Science and Engineering, 217, 012007. doi: https://doi.org/10.1088/1757-899x/217/1/012007

[13] Power, C., McNabola, A., Coughlan, P. (2015). A Parametric Experimental Investigation of the Operating Conditions of Gravitational Vortex Hydropower (GVHP). Journal of Clean Energy Technologies, 4 (2), 112–119. doi: https://doi.org/10.7763/jocet.2016.v4.263

[14] Abbasi, T., Abbasi, S. A. (2011). Small hydro and the environmental implications of its extensive utilization. Renewable and Sustainable Energy Reviews, 15 (4), 2134–2143. doi: https://doi.org/10.1016/j.rser.2010.11.050

[15] Paish, O. (2002). Small hydro power: technology and current status. Renewable and Sustainable Energy Reviews, 6 (6), 537–556. doi: https://doi.org/10.1016/s1364-0321(02)00006-0

[16] Campbell, R. J. (2010). Small Hydro and Low-Head Hydro Power Technologies and Prospects. Available at: https://www.researchgate.net/publication/290980770_Small_hydro_and_low-head_hydro_power_technologies_and_prospects

[17] Bozhinova, S., Hecht, V., Kisliakov, D., Müller, G., Schneider, S. (2013). Hydropower converters with head differences below 2·5 m. Proceedings of the Institution of Civil Engineers – Energy, 166 (3), 107–119. doi: https://doi.org/10.1680/ener.11.00037

[18] Date, A., Akbarzadeh, A. (2009). Design and cost analysis of low head simple reaction hydro turbine for remote area power supply. Renewable Energy, 34 (2), 409–415. doi: https://doi.org/10.1016/j.renene.2008.05.012

[19] Chattha, J. A., Cheema, T. A., Khan, N. H. (2017). Numerical investigation of basin geometries for vortex generation in a gravitational water vortex power plant. 2017 8th International Renewable Energy Congress (IREC). doi: https://doi.org/10.1109/irec.2017.7926028

[20] Marian, B. G.-M., Sajin, T., Florescu, I., Nedelcu, D.-I., Ostahie, C.-N., Catalin (2012). The concept and theorical study of micro hydropower plant with gravitational vortex and turbine with rapidy steps. World energy Syst. Conf. – WESC.

[21] Dhakal, S., Nakarmi, S., Pun, P., Thapa, A. B., Bajracharya, T. R. (2014). Development and Testing of Runner and Conical Basin for Gravitational Water Vortex Power Plant. Journal of the Institute of Engineering, 10 (1), 140–148. doi: https://doi.org/10.3126/jie.v10i1.10895

[22] Dhakal, R. et al. (2017). Runner for Gravitational Water Vortex Power Plant," 6th International Conference on Renewable Energy Research and Applications, 5, 365–373.

[23] Sritram, P., Treedet, W., Suntivarakorn, R. (2015). Effect of turbine materials on power generation efficiency from free water vortex hydro power plant. IOP Conference Series: Materials Science and Engineering, 103, 012018. doi: https://doi.org/10.1088/1757-899x/103/1/012018

[24] Wanchat, S., Suntivarakorn, R., Wanchat, S., Tonmit, K., Kayanyiem, P. (2013). A Parametric Study of a Gravitation Vortex Power Plant. Advanced Materials Research, 805–806, 811–817. doi: https://doi.org/10.4028/www.scientific.net/amr.805-806.811

[25] Mulligan, S., Hull, P. (2010). Design and Optimisation of a Water Vortex Hydropower Plant, 21, 1–21.
[26] Ruiz Sánchez, A., Guevara Muñoz, A. J. (2019). Numerical and Experimental Evaluation of Concave and Convex Designs for Gravitational Water Vortex Turbine. Journal of Advanced Research in Fluid Mechanics and Thermal Sciences, 64 (1), 160–172.
[27] Mathew, S. (2006). Wind energy: Fundamentals, resource analysis and economics. *Berlin: Springer,* 246. doi: http://doi.org/10.1007/3-540-30906-3
[28] Kayastha, M., Raut, P., Kumar, N., Sandesh, S., Ghising, T., Dhakal, R. (2021). CFD evaluation of performance of Gravitational Water Vortex Turbine at different runner positions. KEC Conference, 17–25. doi: http://doi.org/10.31224/osf.io/d9qn3
[29] Anderson, J. D. (1995). Computational fluid dynamics: the basics with applications. McGraw, 547.
[30] Versteeg, H. K., Malalasekera, W. (2007). An introduction to computational fluid dynamics: the finite volume method. New York: Pearson Education, 503.
[31] Munson, B. R., Young, D. F., Okiishi, T. H. (1995). Fundamentals of fluid mechanics. Oceanographic Literature Review, 10 (42), 831. Available at: https://www.infona.pl//resource/bwmeta1.element.elsevier-013ce2bb-5df3-353d-9205-9c4162529c62 Last accessed: 09.12.2021
[32] Alawadhi, E. M. (2020). Meshing guide. Finite Element Simulations Using ANSYS. CRC Press, 407–424. doi: http://doi.org/10.1201/b18949-12
[33] Shashikumar, C. M., Vijaykumar, H., Vasudeva, M. (2021). Numerical investigation of conventional and tapered Savonius hydrokinetic turbines for low-velocity hydropower application in an irrigation channel. Sustainable Energy Technologies and Assessments, 43, 100871. doi: https://doi.org/10.1016/j.seta.2020.100871

*Received date 23.08.2022*
*Accepted date 25.10.2022*
*Published date 29.11.2022*



***How to cite:*** *Burbano, A., Sierra, J., Correa, E., Ruiz, A. Sanin, D. (2022). Numerical simulation of the inlet channel geometry influence in the torque generated at the gravitation water vortex turbine. EUREKA: Physics and Engineering, 6, 106–119. doi: http://doi.org/10.21303/2461-4262.2022.002703*